

Asymmetric Beam Combination for Optical Interferometry

J. D. Monnier

Smithsonian Astrophysical Observatory MS#42, 60 Garden Street, Cambridge, MA, 02138

`jmonnier@cfa.harvard.edu`

ABSTRACT

Optical interferometers increasingly use single-mode fibers as spatial filters to convert varying wavefront distortion into intensity fluctuations which can be monitored for accurate calibration of fringe amplitudes. Here I propose using an *asymmetric* coupler to allow the photometric intensities of each telescope beam to be measured at the same time as the fringe visibility, but without the need for dedicated photometric outputs, which reduce the light throughput in the interferometric channels. In the read-noise limited case often encountered in the infrared, I show that a 53% improvement in signal-to-noise ratio for the visibility amplitude measurement is achievable, when compared to a balanced coupler setup with 50% photometric taps (e.g., the FLUOR experiment). In the Poisson-noise limit appropriate for visible light, the improvement is reduced to only $\sim 8\%$. This scheme also reduces the cost and complexity of the beam combination since fewer components and detectors are required, and can be extended to more than two telescopes for “all-in-one” or pair-wise beam combination. Asymmetric beam combination can also be employed for monitoring scintillation and throughput variations in systems without spatial filtering.

Subject headings: instrumentation: interferometers — techniques: interferometric

1. Introduction

Spatial filtering is key for precise calibration of atmospheric turbulence for ground-based optical interferometers. After sidereal delay compensation, the stellar light from each telescope is focused onto the tip of a single-mode fiber. Up to $\sim 78\%$ of the energy (Shaklan & Roddier 1988) of a perfect telescope beam can be coupled into a single-mode fiber. In practice, this coupling efficiency is significantly less, depending on how well the incoming electric field distribution overlaps with the fiber beam profile. This is the act of “spatial filtering,” whereby only the “clean” part of each wavefront (one spatial mode) is transmitted by the single-mode fiber. In essence, phase irregularities of the incoming wavefronts are converted into amplitude fluctuations, trading a difficult to measure quantity for one easily monitored (e.g., Shaklan 1989).

The light from each fiber can then be efficiently and coherently combined in a balanced 2x2 coupler, a fiber optic component which mixes 50% of the light from each telescope coherently,

equivalent to a beamsplitter. In some cases, approximately one-half the light is split-off from each fiber before the coupler to act as a “photometric tap,” a direct and real-time monitor of the coupling efficiency for each telescope. In this scheme the fringe amplitude measured at the outputs of the coupler can be directly calibrated based on the strength of the signals in the photometric taps (e.g., Coude Du Foresto et al. 1997).

There are two distinct ways that spatial filtering improves calibration. The most important effect is that the *mean coupling* into each fiber is a direct measure of atmospheric turbulence, with poor seeing resulting in low coupling efficiency. When seeing inevitably changes in the time between observing the target and calibrator, the coupling efficiency into the fibers will change, and this will be seen as a change in average signal level. However, since the interference efficiency in the 2x2 coupler is not a function of atmospheric conditions, the overall calibration of the system visibility is maintained. Heterodyne detection is another kind of spatial filtering which utilizes this principle, and is one reason why the Infrared Spatial Interferometer (e.g., Hale et al. 2000) can maintain accurate calibration despite the dearth of bright mid-infrared calibrators.

The second way spatial filtering can improve measurement precision is by correcting for short-term fluctuations in coupling efficiency. The fringe amplitude is proportional to the harmonic mean of the two telescope intensity levels (e.g., see Eq. 3), while the DC level is proportional to the sum of the two telescope intensity levels. This means that the fringe contrast, or visibility, decreases when the signal from one telescope is significantly greater than the other. While this effect on the system visibility can be statistically calibrated by using a calibrator star, the use of photometric taps allows each individual fringe measurement to be independently calibrated. This second use of spatial filtering allows high quality fringe visibility estimates with very few measurements, since one does not have to statistically average over these fluctuations (for specific application and discussion, see Coude Du Foresto et al. 1997). Note that this second aspect of spatial filtering is of limited utility for faint sources, since it can only be applied when the signal levels can be measured to reasonable accuracy within a single atmospheric coherence time.

Initial experiments using spatial filters in infrared interferometry have led to dramatic improvement in the precision of visibility measurements. Using fluoride single-mode fibers with in-line 2x2 couplers and photometric taps, Perrin et al. (1999) have reported visibility measurements with 0.3% precision of bright M-giants in the K-band, 10 to 20× better than the precision reported using traditional techniques (e.g., Dyck et al. 1996; Nordgren et al. 1999).

In this short paper, I discuss the use of *asymmetric* 2x2 couplers which can permit the calibration improvements derived from photometric taps but without diverting valuable photons from the fringe amplitude measurement. I will detail the signal-to-noise ratio advantages in both read-noise and Poisson-noise limiting cases. Lastly, I will briefly comment on how these ideas can be applied to other beam combination schemes, such as when spatial filtering occurs *after* beam combination, for pair-wise and “all-in-one” combiners for more than two beams, for free-space combiners with no spatial filtering, and for fringe-tracking systems.

2. Balanced and Asymmetric Couplers

As mentioned in the Introduction, current fiber optic correlators, e.g. FLUOR instrument on the IOTA interferometer (Coude Du Foresto et al. 1997), VINCI on VLTI (Foresto, private communication), use a photometric tap which removes $\sim 50\%$ of the light from each telescope before beam combination in a “Balanced” (symmetric 50/50) coupler (hereafter, “B-coupler”). This is schematically indicated in the top panel of Figure 1. However, this method is not efficient for resolved or faint sources since roughly half the photons are being diverted from the fringe measurement for the photometry; it is clearly futile to monitor photometric fluctuations when the fringes can not even be detected.

The bottom panel of Figure 1 shows a novel method for recovering the photometric signals without requiring dedicated photometric taps, thus allowing improved sensitivity while maintaining high calibration precision. At the center of the design is an “Asymmetric” coupler (hereafter, “A-coupler”). An A-coupler is much like a beamsplitter manufactured to reflect a different fraction than it transmits. It will be shown that the photometric signals from each telescope can be reconstructed through appropriate linear combinations of the interferometric signals after the A-coupler, assuming the properties of the coupler are well-known. While the fringe contrast from an A-coupler is slightly decreased by having unequal contributions from each telescopes, the signal strength is increased since no light is wasted on dedicated photometric taps.

For the following discussion and calculations I will refer to Figure 1 which labels the various input and outputs to the beam combiners under consideration. The incident photon fluxes (photons \cdot s $^{-1}$) coming from telescope 1 and 2 will be denoted as F_1 and F_2 respectively. In order to take into account the finite quantum efficiency η of the detector, substitute ηF_i for F_i in the subsequent formulas. Both combiners under consideration (“B-Coupler” and “A-Coupler”) have so-called “interferometric outputs,” labeled I_1 and I_2 , while the “B-Coupler” also has two photometric outputs P_1 and P_2 .

For this calculation we will assume idealized systems. The B-coupler scheme will divert 50% of the incident light into the photometric channels, and we will also assume the coupler is exactly balanced and loss-less. Under these assumptions the output signals can be expressed as:

$$P_1 = \frac{F_1}{2} \tag{1}$$

$$P_2 = \frac{F_2}{2} \tag{2}$$

$$I_1 = \frac{F_1}{4} + \frac{F_2}{4} + 2\sqrt{\frac{F_1}{4} \frac{F_2}{4}}\gamma(t) = \frac{F_1}{4} + \frac{F_2}{4} + \frac{1}{2}\sqrt{F_1 F_2}\gamma(t) \tag{3}$$

$$I_2 = \frac{F_1}{4} + \frac{F_2}{4} - 2\sqrt{\frac{F_1}{4} \frac{F_2}{4}}\gamma(t) = \frac{F_1}{4} + \frac{F_2}{4} - \frac{1}{2}\sqrt{F_1 F_2}\gamma(t) \tag{4}$$

In the last two equations, $\gamma(t)$ is the mutual coherence function and encodes the fringe visibility,

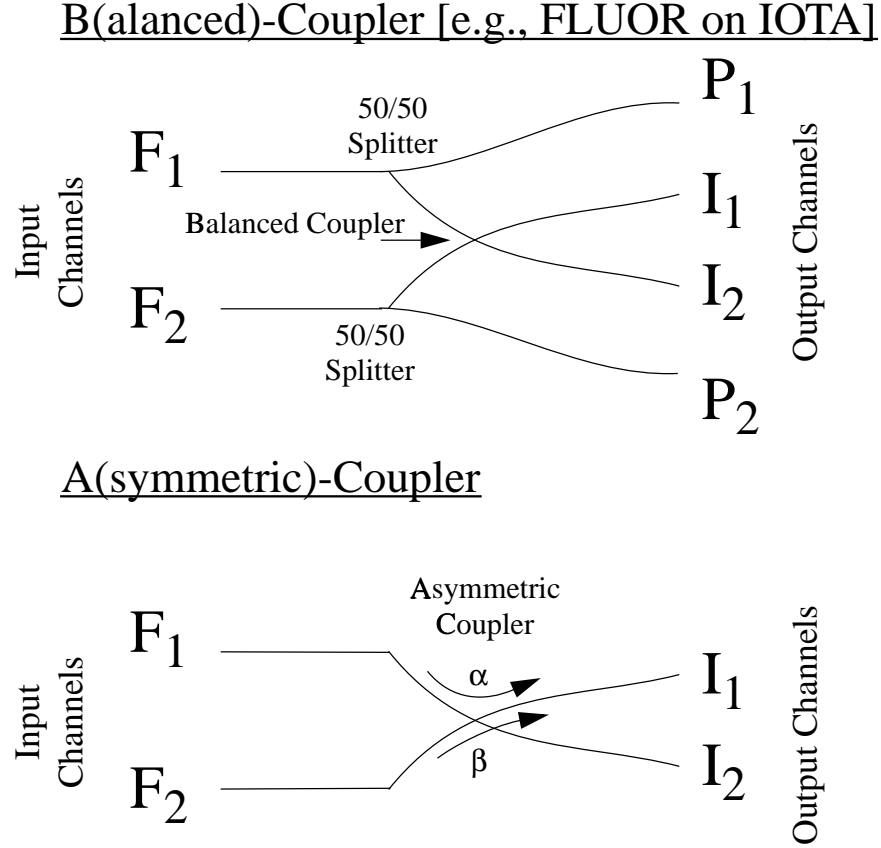


Fig. 1.— This diagram illustrates the basic designs of the FLUOR-type (Balanced) Coupler and the Asymmetric coupler design, being proposed here. F_1 and F_2 represent the incoming fluxes from telescopes 1 and 2. (*top panel*) B(alanced)-coupler design shows a 50% photometric tap before the remaining light from each telescope is combined in a 50/50 (balanced, or symmetric) coupler. P_1 and P_2 correspond to the photometric channels, while the interferometric channels, I_1 and I_2 , contain the optical fringes. (*bottom panel*) There are no photometric channels in this design, but rather an Asymmetric coupler is used to combine the light. As shown in the figure, the fraction α (β) of F_1 (F_2) appear at I_1 , while the fraction β (α) of F_1 (F_2) appear at I_2 .

the quantity we wish to measure. Usually γ is temporally modulated by adjusting the relative path lengths in the two arms of the interferometer; this will be discussed further when we calculate the signal-to-noise ratios for the different coupler designs.

The A-coupler will be defined so that the fraction α of F_1 is mixed with β of F_2 for interferometric output channel I_1 , while the fraction β of F_1 is mixed with fraction α of F_2 for interference in I_2 . If the coupler is loss-less, then $\beta = 1 - \alpha$, but I will keep the α and β notation for equation simplicity. To summarize, the outputs of the A-coupler are given as:

$$I_1 = \alpha F_1 + \beta F_2 + 2\sqrt{\alpha F_1 \beta F_2} \cdot \gamma(t) \quad (5)$$

$$I_2 = \beta F_1 + \alpha F_2 - 2\sqrt{\alpha F_1 \beta F_2} \cdot \gamma(t) \quad (6)$$

2.1. Determining photometric signals with A-coupler

While determination of F_1 and F_2 is straightforward for the case of the B-coupler (see Eqs. 1 & 2), let us now discuss how to retrieve this same information using the A-coupler. We can split the I_i signal into the sum of an incoherent and a coherent term, $I = I_{\text{incoherent}} + I_{\text{coherent}}$. The coherent part of this equation contains the interferometric “fringe” signal, and is usually separated from the incoherent part by temporal modulation of $\gamma(t)$ at a frequency ν greater than $\frac{1}{\tau_0}$, where τ_0 is the coherence time of the atmosphere. In order to estimate the photometric flux from each telescope at the same time as we are detecting the fringe we must be able to estimate the incoherent part of the I -channels. For the rest of this discussion, we will denote this incoherent component of the I -channels as $\langle I_i \rangle$, where the time-averaging is sufficient to remove the fringe component but not atmospheric fluctuations; this is equivalent to setting $\gamma(t) = 0$ in Eqs. (5) and (6). The following SNR calculations for the A-coupler do assume one can separate the coherent and incoherent parts perfectly.

In order to estimate F_i using the A-coupler scheme we must use linear combinations of $\langle I_1 \rangle$ and $\langle I_2 \rangle$. From inspection of Eqs. (5) and (6), we see that:

$$F_1 = \frac{\alpha \langle I_1 \rangle - \beta \langle I_2 \rangle}{\alpha^2 - \beta^2} \quad (7)$$

$$F_2 = \frac{\beta \langle I_1 \rangle - \alpha \langle I_2 \rangle}{\beta^2 - \alpha^2} \quad (8)$$

Note that these equations become indeterminate when $\alpha = \beta$, corresponding to the balanced coupler case, $\alpha = \frac{1}{2}$. This tells us that α must be significantly larger than β in order to avoid “amplifying” the measurement uncertainty when estimating F_i .

3. Signal-to-Noise Ratio Calculation

In this section, I will compare the Signal-to-Noise Ratio (SNR) for the proposed asymmetric coupler system (A-coupler) versus the traditional setup using a 50% photometric tap and balanced couplers for the interference (B-coupler).

3.1. Read-Noise Limit (Infrared)

In the read-noise limited situation, we can imagine each output channel having the same read-noise σ_{read} . Since the B-coupler scheme has twice the number of output channels, we see that more read-noise is introduced and we can expect degraded SNR. In the case of background-limited observations, the considerations are similar to the read-noise dominated case, since read-noise and background noise are both independent of signal strength and average as the root of the number of independent measurements. However, the discussion is complicated since background radiation

can originate both before and after the combiner. The background-limited case is discussed briefly in §3.3.

We proceed to calculate the SNR for the read-noise limited case.

3.1.1. Photometric Channels

The amplitudes of the photometric and interferometric signals were determined in §2 (Eq.1-8). For the B-coupler, the noise in each photometric channel is obviously σ_{read} per sample. For a total integration time of $N \Delta t$ (N samples each with integration time of Δt), it is trivial to calculate the estimated signal-to-noise ratio (SNR) and this result has been placed in Table 1.

For the A-coupler we form the linear combination described in §2.1, Eqs. (7) and (8). In estimating F_i we must combine the errors from $\langle I_1 \rangle$ and $\langle I_2 \rangle$ in quadrature, weighted by the appropriate factors. Let us also assume here we are averaging N separate samples, each with integration time of Δt , to take into account averaging over the fringe modulation (see §2.1). In this case, the SNR for F_1 can be written as:

$$\text{SNR } F_1 \equiv \frac{\text{Signal}}{\text{Noise}} = \frac{F_1 N \Delta t}{\frac{\sqrt{N} \sigma_{\text{read}} \sqrt{\alpha^2 + \beta^2}}{|\alpha^2 - \beta^2|}} \quad (9)$$

$$= \frac{|\alpha^2 - \beta^2| F_1 \sqrt{N} \Delta t}{\sigma_{\text{read}} \sqrt{\alpha^2 + \beta^2}} \quad (10)$$

A similar derivation for F_2 completes the first half of Table 1.

3.1.2. Interferometric Channels

It is more straightforward to calculate the SNR for the fringe amplitude. The signal strength is simply equal to the coherent term of I_i , while the noise per sample is σ_{read} . Eq. (5) can be used to calculate the signal-to-noise ratio for Fringe 1 as follows:

$$\text{SNR Fringe 1} \equiv \frac{\text{Coherent part of } I_1}{\text{Read Noise}} = \frac{2N \Delta t \sqrt{\alpha F_1 \beta F_2} |\gamma|}{\sigma_{\text{read}} \sqrt{N}} \quad (11)$$

$$= \frac{2\sqrt{N} \Delta t}{\sigma_{\text{read}}} \sqrt{\alpha F_1 \beta F_2} |\gamma| \quad (12)$$

Substituting $\alpha = \beta = \frac{1}{4}$, this result can be applied for the case of B-coupler. These results now appear in Table 1.

The SNR advantage of the A-coupler approach, $\text{SNRA} = \frac{\text{A-Coupler SNR}}{\text{B-Coupler SNR}}$, has been included in the last column of Table 1 and will be discussed in §3.3.

Table 1: Signal-to-Noise Ratio Comparison: Read-Noise Limited

Quantity to be Estimated	B-Coupler SNR	A-Coupler SNR	SNR Advantage of A-Coupler over B-Coupler
F_1	$\frac{F_1\sqrt{N}\Delta t}{2\sigma_{\text{read}}}$	$\frac{ \alpha^2-\beta^2 F_1\sqrt{N}\Delta t}{\sigma_{\text{read}}\sqrt{\alpha^2+\beta^2}}$	$\frac{2 \alpha^2-\beta^2 }{\sqrt{\alpha^2+\beta^2}}$
F_2	$\frac{F_2\sqrt{N}\Delta t}{2\sigma_{\text{read}}}$	$\frac{ \beta^2-\alpha^2 F_2\sqrt{N}\Delta t}{\sigma_{\text{read}}\sqrt{\beta^2+\alpha^2}}$	$\frac{2 \alpha^2-\beta^2 }{\sqrt{\alpha^2+\beta^2}}$
I_1 Fringe	$\frac{\sqrt{N}\Delta t}{2\sigma_{\text{read}}}\sqrt{F_1F_2} \gamma $	$\frac{2\sqrt{N}\Delta t}{\sigma_{\text{read}}}\sqrt{\alpha F_1\beta F_2} \gamma $	$4\sqrt{\alpha\beta}$
I_2 Fringe	$\frac{\sqrt{N}\Delta t}{2\sigma_{\text{read}}}\sqrt{F_1F_2} \gamma $	$\frac{2\sqrt{N}\Delta t}{\sigma_{\text{read}}}\sqrt{\alpha F_1\beta F_2} \gamma $	$4\sqrt{\alpha\beta}$

3.2. Photon-Noise Limit (Visible)

In the photon-limited regime, there is no explicit punishment for using extra detectors or for multiple reads, and therefore we do not expect the A-coupler advantage to be as significant here. We will keep all the other notation the same. The formulation for SNR for A- and B-couplers developed in the last section still applies, except we must use σ_{photon} instead of σ_{read} . For pure Poisson noise, the rms fluctuation in the measurement of $F_1N\Delta t$ photons is simply $\sqrt{F_1N\Delta t}$ photons. We now proceed to create Table 2 containing the SNR for the B-coupler and A-coupler under photon-noise dominated conditions.

3.2.1. Photometric Channels

For the B-coupler, the noise in each photometric channel is equal to the square root of the number of detected photons. For a total integration time of $N\Delta t$, the estimated SNR is straightforward to derive, and appears in Table 2.

As before, use of the A-coupler requires the formation of linear combinations (Eqs. 7 and 8) of $\langle I_1 \rangle$ and $\langle I_2 \rangle$ to estimate F_i . To correctly propagate the measurement uncertainties of $\langle I_1 \rangle$ and $\langle I_2 \rangle$ into our estimate of F_i , we combine the Poisson errors from $\langle I_1 \rangle$ and $\langle I_2 \rangle$ in quadrature, weighted by the appropriate factors. As before, we average N separate samples, each with integration time of Δt , to take into account averaging over the fringe modulation. In this case, the SNR for F_1 can be written as:

$$\text{SNR } F_1 \equiv \frac{\text{Signal}}{\text{Noise}} = \frac{F_1 N \Delta t}{\left[\left(\alpha \sqrt{\langle I_1 \rangle N \Delta t} \right)^2 + \left(\beta \sqrt{\langle I_2 \rangle N \Delta t} \right)^2 \right]^{\frac{1}{2}}} \quad (13)$$

$$= \frac{F_1 \sqrt{N \Delta t}}{\frac{\sqrt{\alpha^2(\alpha F_1 + \beta F_2) + \beta^2(\beta F_1 + \alpha F_2)}}{|\alpha^2 - \beta^2|}} \quad (14)$$

$$= \frac{|\alpha^2 - \beta^2| F_1 \sqrt{N \Delta t}}{\sqrt{\alpha^2(\alpha F_1 + \beta F_2) + \beta^2(\beta F_1 + \alpha F_2)}} \quad (15)$$

I have not collected terms further in order to make it more apparent that for the nominal case of a loss-less coupler ($\alpha + \beta = 1$) and for equal fluxes from each telescope ($\langle F_1 \rangle = \langle F_2 \rangle$), then $\text{SNR } F_1 = \frac{|\alpha^2 - \beta^2| \sqrt{F_1 N \Delta t}}{\sqrt{\alpha^2 + \beta^2}}$, which has the same (α, β) dependences as for the read-noise limited case (see Eq. 10). The calculation for $\text{SNR } F_2$ follows directly, and we place these results in Table 2.

3.2.2. Interferometric Channels

As for the read-noise limited case, the SNR of the fringe amplitude is more straightforward to derive than for the photometric signals. The signal strength is simply equal to the *coherent term* of I_i , while the Poisson noise should be calculated based on the *incoherent term* $\langle I_i \rangle$, corresponding to the average flux. Eq. (5) can be used to calculate the signal-to-noise ratio for Fringe 1 as follows:

$$\text{SNR Fringe 1} \equiv \frac{\text{Coherent part of } I_1}{\text{Poisson Noise of } \langle I_1 \rangle} = \frac{2N\Delta t \sqrt{\alpha F_1 \beta F_2} |\gamma|}{\sqrt{(\alpha F_1 + \beta F_2) N \Delta t}} \quad (16)$$

$$= \frac{2\sqrt{N\Delta t} \sqrt{\alpha F_1 \beta F_2} |\gamma|}{\sqrt{(\alpha F_1 + \beta F_2)}} \quad (17)$$

This result also applies for the B-combiner, substituting $\alpha = \beta = \frac{1}{4}$.

As for the photometric SNR using the A-coupler, this result (Eq. 17) can be greatly simplified in the case of a loss-less combiner and equal telescope fluxes, i.e. $\text{SNR Fringe 1} = 2\sqrt{F_1 N \Delta t} \sqrt{\alpha \beta} |\gamma|$, which has the same (α, β) dependence as the read-noise limited case.

3.3. Comparison

In order to facilitate comparison between the performance of the A-coupler and the B-coupler, we will make a few simplifying assumptions. We will assume that $\langle F_1 \rangle = \langle F_2 \rangle$ and that the A-coupler is loss-less ($\alpha + \beta = 1$). In addition, we will introduce a new quantity, $A = \frac{\alpha}{\beta}$, the ‘‘Asymmetry Factor,’’ defined greater than or equal to unity. Note that for a balanced system, the Asymmetry Factor is equal to Unity.

For this simplified configuration, the SNRs for the two photometric determinations are identical, as are the SNRs for Fringes 1 and Fringes 2. Therefore, we will stop differentiating between the two and speak only of the SNR of the photometric signal (i.e., the flux amplitude) and of the interferometric signal (i.e., the fringe amplitude). Table 3 contains the SNR advantage of the A-coupler over the B-coupler as a function for Asymmetry Factor (A) for the read-noise and photon-noise limit cases based on results contained in the Tables 1 and 2. Note that the SNR advantage between

Table 2: Signal-to-Noise Ratio Comparison: Photon-Noise Limited

Quantity to be Estimated	B-Coupler SNR	A-Coupler SNR	SNR Advantage of A-Coupler over B-Coupler
F_1	$\sqrt{\frac{F_1 N \Delta t}{2}}$	$\frac{ \alpha^2 - \beta^2 F_1 \sqrt{N \Delta t}}{\sqrt{\alpha^2(\alpha F_1 + \beta F_2) + \beta^2(\beta F_1 + \alpha F_2)}}$	$\frac{\sqrt{2} \alpha^2 - \beta^2 }{\sqrt{\alpha^2\left(\alpha + \beta \frac{F_2}{F_1}\right) + \beta^2\left(\beta + \alpha \frac{F_2}{F_1}\right)}}$
F_2	$\sqrt{\frac{F_2 N \Delta t}{2}}$	$\frac{ \beta^2 - \alpha^2 F_2 \sqrt{N \Delta t}}{\sqrt{\beta^2(\alpha F_1 + \beta F_2) + \alpha^2(\beta F_1 + \alpha F_2)}}$	$\frac{\sqrt{2} \alpha^2 - \beta^2 }{\sqrt{\alpha^2\left(\alpha + \beta \frac{F_1}{F_2}\right) + \beta^2\left(\beta + \alpha \frac{F_1}{F_2}\right)}}$
I_1 Fringe	$\frac{\sqrt{N \Delta t} F_1 F_2 \gamma }{\sqrt{F_1 + F_2}}$	$\frac{2\sqrt{N \Delta t} \alpha \beta F_1 F_2 \gamma }{\sqrt{(\alpha F_1 + \beta F_2)}}$	$2\sqrt{\alpha \beta} \sqrt{\frac{1 + \frac{F_2}{F_1}}{\alpha + \beta \frac{F_2}{F_1}}}$
I_2 Fringe	$\frac{\sqrt{N \Delta t} F_1 F_2 \gamma }{\sqrt{F_1 + F_2}}$	$\frac{2\sqrt{N \Delta t} \alpha \beta F_1 F_2 \gamma }{\sqrt{(\beta F_1 + \alpha F_2)}}$	$2\sqrt{\alpha \beta} \sqrt{\frac{1 + \frac{F_1}{F_2}}{\alpha + \beta \frac{F_1}{F_2}}}$

the read-noise-limited and photon-limited regimes differs by exactly $\sqrt{2}$ for both the flux and the fringe amplitude estimators.

It is interesting to note that the background-limited case falls somewhere in-between these two limits. The photometric channels and the non-unity coupling efficiency will introduce background radiation at the temperature of the fiber optic components. For a free-space system, this is equivalent to the fact that you can not “split-off” a fraction of a beam without introducing new lines-of-sight to the detector not coupled to the sky; thus additional background degrades the measurement. However if the combiner is cryogenically cooled, the background-limited case will be identical to the photon-noise limited case. Alternatively, if emission from the combiner dominates sky+telescope emission then the background-limited case will share the same SNR as the read-noise limited case. In practice, the result will intermediate.

If we assume the SNRs of the flux amplitude and fringe amplitude are equally important for estimating the fringe visibility (or contrast), which is probably only true for relatively bright sources, then we can estimate the combined SNR Advantage (SNRA) of the A-coupler over the B-coupler by applying equal weights and adding the errors in quadrature. Mathematically, this is done as follows:

$$SNRA_{\text{visibility}} \equiv \frac{\sqrt{2}}{\sqrt{\frac{1}{SNRA_{\text{Flux}}^2} + \frac{1}{SNRA_{\text{Fringe}}^2}}} \quad (18)$$

These results are shown graphically in Figures 2 and 3. In the read-noise limited case, we see that the A-coupler design is superior for Asymmetry factors greater than 1.78 and less than 25.63, with maximum improvement of 53% for $A = 4.61$. In the photon-noise limit, the A-coupler is only slightly superior between Asymmetry factors of 2.82 and 8.71, with a maximum improvement of

Table 3: Summary: Signal-to-Noise Ratio as Function of Asymmetry Factor A

Quantity to be Estimated	SNR Advantage of A-Coupler over B-Coupler	
	[Read-Noise Limit]	[Photon-Noise Limit]
Flux Amplitude	$2 \frac{(A-1)}{\sqrt{A^2+1}}$	$\sqrt{2} \frac{(A-1)}{\sqrt{A^2+1}}$
Fringe Amplitude	$4 \frac{\sqrt{A}}{A+1}$	$2\sqrt{2} \frac{\sqrt{A}}{A+1}$

8.2%, also at $A = 4.61$.

Strictly speaking, the photometric signal can be averaged for longer than the fringes since the fringes must be modulated faster than the atmospheric time scale. This means that the SNR of the B-coupler setup can be improved by diverting a smaller percentage of the flux to the photometric taps; the optimal ratio would depend on various instrumental and observing factors, such as the inherent fringe visibility of your source and the temporal coherence time of the atmosphere. However by the same argument, the SNR of the A-coupler setup can be also improved by using a smaller asymmetry factor. These details have been neglected in the above calculation, but are not expected to qualitatively change the results.

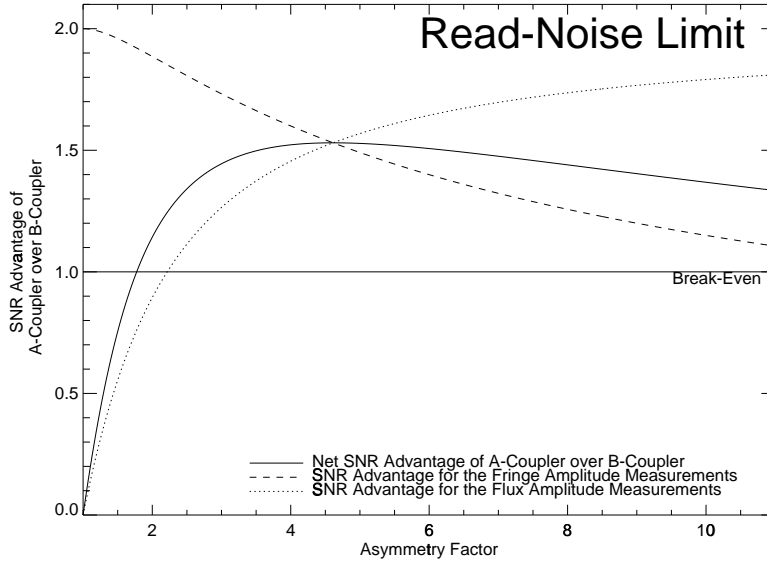


Fig. 2.— Signal-to-Noise Ratio Advantage for Asymmetric-Coupler over Balanced Coupler, as a function of the A-coupler Asymmetry Factor, assuming read-noise limited performance.

4. Discussion

We see that the A-coupler offers a significant improvement for the read-noise limited case, and a slight improvement in the photon-noise limit. This method will work with a FLUOR-type system where beam combination occurs in a fiber optic coupler or integrated optic (Berger et al. 1999). Fringe-tracking systems can benefit from this scheme as well, since the mean signal in each interferometric channel can be separately determined by binning all data in each fringe-modulation period, but this does require *both* interferometric channels to be measured simultaneously. Asymmetric beam combination is also useful when there is no spatial filtering. Other effects can cause modulation of the beam intensities from telescopes, including scintillation and guiding errors, and the methods outlined here can be used to correct for these effects.

For interferometric arrays with three or more telescopes, other possibilities exist for determining the individual telescope photometric strengths. The A-coupler scheme can be generalized for “all-in-one” combiners (e.g., Baldwin et al. 1994), for instance using four asymmetric couplers allows one to differentiate the four input signals using the four output signals. Interestingly for the three-telescope (or more) pair-wise combination scheme, the photometric signals can be determined even with standard, symmetric couplers using linear combinations similar to the ones derived here.

Another advantage to the A-coupler design is decreased complexity of the combiner, although the data analysis will be more complicated. This is especially important in the visible, because of the expensive cost of high quantum efficiency, photon-counting detectors, such as avalanche photo-diodes (APDs). One apparent disadvantage to an A-coupler design is that one can no longer subtract the two interferometric signals to remove “common-mode” fluctuations such as scintillation. However, when the fringes are modulated faster than scintillation time scales, these variations can be completely corrected by forming the appropriate linear combinations as already discussed herein.

One caveat should be mentioned here. When spatial filtering occurs after (free-space) beam combination (e.g., Colavita et al. 1999), these methods may not work well. The reason is that optical misalignments leading to the single-mode fibers can cause decorrelations between the coupling efficiencies on either side of the free-space beamsplitter. For instance, a wavefront tilt introduced by the atmosphere could cause an increase in coupling efficiency for one fiber, but a decrease for the other fiber if the optical axes of both fibers are not aligned identically with the telescope axis. Hence, the photometric estimators will not be a fixed linear combination of the interferometric outputs, degrading the utility of the technique.

An experiment is underway at the Harvard-Smithsonian Center for Astrophysics to test these ideas, using a 780 nm asymmetric coupler, asymmetry factor 2.3. If lab tests prove satisfactory, the equipment will be incorporated into IOTA (Carleton et al. 1994), utilizing much of the existing visible light detection system for measurements of stellar diameters. The ultimate goal of this experiment is to yield high precision diameters measurements ($\ll 1\%$), allowing the pulsation amplitude to be measured for calibration of the Cepheid distance scale.

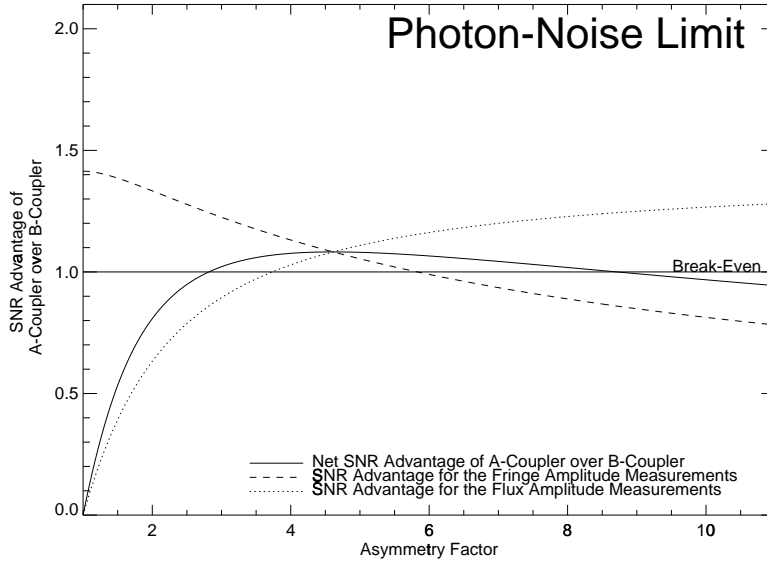


Fig. 3.— Signal-to-Noise Ratio Advantage for Asymmetric-Coupler over Balanced Coupler, as a function of the A-coupler Asymmetry Factor, assuming photon-noise limited performance.

5. Conclusions

Asymmetric beam combination in optical interferometry can improve sensitivity while reducing combiner complexity and cost, especially in the read-noise limited regime encountered for most infrared observing.

I appreciate discussions with Rafael Millan-Gabet, Jean-Phillipe Berger, Wes Traub, and other IOTA group members, and thank Peter Tuthill and David Mozurkewich for comments on the manuscript. Nat Carleton pointed out how photometric correction for a three-telescope, pair-wise combination scheme can be achieved with symmetric couplers, using appropriate linear combinations of the output channels. After the manuscript was submitted, the author was informed that a similar idea was proposed in 1995 by Jean Gay of Observatoire de la Cote d’Azur in Nice. JDM acknowledges support from a Center for Astrophysics Fellowship at the Harvard-Smithsonian Center for Astrophysics.

REFERENCES

- Baldwin, J. E., Boysen, R. C., Cox, G. C., Haniff, C. A., Rogers, J., Warner, P. J., Wilson, D. M., & Mackay, C. D. 1994, Proc. SPIE, 2200, 118

- Berger, J. P., Rousselet-Perraut, K., Kern, P., Malbet, F., Schanen-Duport, I., Reynaud, F., Haguenaer, P., & Benech, P. 1999, *A&AS*, 139, 173
- Carleton, N. P., Traub, W. A., Lacasse, M. G., Nisenson, P., Pearlman, M. R., Reasenber, R. D., Xu, X., Coldwell, C. M., Panasyuk, A., Benson, J. A., Papaliolios, C., Predmore, R., Schloerb, F. P., Dyck, H. M., & Gibson, D. M. 1994, *Proc. SPIE*, 2200, 152
- Colavita, M. M., Wallace, J. K., Hines, B. E., Gursel, Y., Malbet, F., Palmer, D. L., Pan, X. P., Shao, M., Yu, J. W., Boden, A. F., Dumont, P. J., Gubler, J., Koresko, C. D., Kulkarni, S. R., Lane, B. F., Mobley, D. W., & van Belle, G. T. 1999, *ApJ*, 510, 505
- Coude Du Foresto, V., Ridgway, S., & Mariotti, J. . 1997, *A&AS*, 121, 379
- Dyck, H. M., Benson, J. A., Van Belle, G. T., & Ridgway, S. T. 1996, *AJ*, 111, 1705+
- Hale, D. D. S., Bester, M., Danchi, W. C., Fitelson, W., Hoss, S., Lipman, E. A., Monnier, J. D., Tuthill, P. G., & Townes, C. H. 2000, *ApJ*, 537, 998
- Nordgren, T. E., Germain, M. E., Benson, J. A., Mozurkewich, D., Sudol, J. J., Elias, N. M., Hajian, A. R., White, N. M., Hutter, D. J., Johnston, K. J., Gauss, F. S., Armstrong, J. T., Pauls, T. A., & Rickard, L. J. 1999, *AJ*, 118, 3032
- Perrin, G., Foresto, V. C. ., Ridgway, S. T., Mennesson, B., Ruilier, C., Mariotti, J. ., Traub, W. A., & Lacasse, M. G. 1999, *A&A*, 345, 221
- Shaklan, S. & Roddier, F. 1988, *Appl. Opt.*, 27, 2334
- Shaklan, S. B. 1989, PhD thesis, The University of Arizona